RESEARCH ON OPTIMAL TORSIONAL DEFORMATION OF FLAPPING WING

Jiayuan Liu[1], Dong Xue[1,2,*]

[1] School of Aeronautics, Northwestern Polytechnical University, Xi'an 710072, China

[2] National Key Laboratory of Aircraft Configuration Design, Xi'an, 710072, PR China

Abstract

When in flight, the wings of a living organism are often subject to a certain amount of torsional movement, especially during the climbing phase when significant thrust is required. Therefore, the appropriate twisting motion of the wings can enhance the thrust performance. The "Dove" biomimetic flapping-wing micro aerial vehicles of Northwestern Polytechnical University achieves passive torsional motion during flight through wing flexibility. The research focuses on the "Dove" wing. experiments and numerical simulations are conducted on its cruising state to verify whether the wing's stiffness distribution reaches the optimal torsional state. An experiment and numerical simulation were conducted to verify whether the rigid distribution of the wing reached the optimal torsional state by testing and modeling its cruising conditions. The experimental study on the wing of the "Dove" was conducted using high-speed camera technology in this paper, and the twisting states of six different spanwise positions, SP_1-SP_6, were obtained by employing the Direct Linear Transformation (DLT) method. The experimental results indicate that the further the spanwise position is from the flapping axis, the greater the torsional deformation it generates. Additionally, due to the influence of inertia forces present in the wings, the peak of torsion occurs earlier than the mid time of downstroke and upstroke. The geometric and kinematic parameters of the selected "Dove" wing span positions SP_1-SP_6 are extracted and calculated using the RANS method for the two-dimensional wing profiles at each span position at various pitch amplitudes of heave pitching motion. The geometric and kinematic parameters of the selected "Dove" wing span positions SP_1-SP_6 are extracted. The two-dimensional airfoil at each spanwise position is subjected to calculations of heave and pitch motions with varying pitch amplitudes using the RANS method. The calculation results of different pitch amplitudes are compared, and the pitch amplitude corresponding to the maximum thrust is defined as the optimal pitch angle. The twist state of the current "Dove" wing obtained from experiments is compared with the optimal pitch angle obtained from numerical simulations, revealing that the twist deformation near the wing root is closer to the optimal pitch angle, while the twist deformation near the wingtip is too large. Therefore, the stiffness distribution of the "Dove" wing near the wing root is considered more appropriate, while stiffness near the wingtip needs to be appropriately increased to reduce the twist amplitude at the wingtip. This study examined the influences of incoming velocity, frequency, and heave amplitude on the optimal pitch angle. It was found that frequency and heave amplitude were positively correlated with the optimal pitch angle, while incoming velocity was negatively correlated with the optimal pitch angle. It is worth noting that the magnitude of the effective angle of attack is collectively controlled by incoming velocity, frequency, heave amplitude, and pitch amplitude. The variation of the optimal pitch angle with incoming velocity, frequency, and heave amplitude can avoid excessively large or small effective angle of attack magnitudes, thereby achieving maximum thrust.

Keywords: high-speed camera technology, torsional deformation, thrust, the optimal pitch angle, stiffness distribution

1. Introduction

Close observation of flying organisms reveals that their wing movements often generate a certain degree of torsional motion, especially during the climbing flight phase where significant thrust is generated. Baier[1] through quasi-steady and unsteady analysis, found that the mechanical energy generated by the flapping motion of the wings can be converted into thrust through a process of chordwise torsion. Therefore, for Biomimetic Flapping-wing Micro Aerial Vehicles (BFMAVs) inspired by birds, appropriate torsional motion will result in better thrust performance, which can be achieved through either active torsion control techniques or passive torsion mechanisms. At present, most BFMAVs achieve passive torsional motion through wing flexibility, such as the "Dove" aircraft developed by Northwestern Polytechnical University[2]. Some aircraft employ active torsion control techniques, such as the Smartbird[3], a flapping-wing unmanned aerial vehicle equipped with torsional actuators at its wingtips. However, due to the significant power consumption associated with active torsion, the overall efficiency improvement is often not substantial. Therefore, selecting an appropriate passive torsional range can better enhance the performance of flapping-wing aircraft.

Currently, research has shown that torsional motion has a certain influence on thrust. Jiao[4] and Chowdhury[5] based on analytical methods, studied the relationship between the coupled flapping-torsional motion of wings during horizontal flight and thrust generation, thus achieving forward thrust-constrained wing design. Küssner[6] and Theodorsen[7] proposed unsteady methods to solve the aerodynamics of flapping wings, indicating that the thrust generated by flapping wings is converted with the assistance of both flapping and torsional motions.

From a two-dimensional perspective, the flapping motion and passive twisting motion of a flapping wing are observed. The flapping motion manifests as the heaving motion of the wing shape at different spanwise positions, while the twisting motion manifests as the passive pitching motion of the wing shape at different spanwise positions. There are more studies exploring the effect of different parameters on aerodynamic performance based on two-dimensional airfoils. Lu[8] investigated the small effect of different rigid airfoils in two dimensions on the time-averaged thrust. The pitch motion amplitude has a positive effect on both average thrust and average power. Furthermore, as the duration of the maximum value of non-sinusoidal motion increases, both average thrust and average power also increase. Lagopoulos et al.[9] investigated the heave-pitch motion of a two-dimensional rigid wing and found that drag can be converted into thrust. The study by Fernandez et al.[10] indicated that the propulsive efficiency of an airfoil is greatest when the pitch center is located near the one-quarter chord length from the leading edge. In contrast, when the pitching center is located between the three-quarter chord point and the trailing edge, no thrust is generated.

In this study, the heaving and pitching motions of two-dimensional airfoils with different geometrical and kinematic parameters are analyzed, and the optimal heaving and pitching motions of flapping wings in various spanwise positions are obtained under specific working conditions to obtain the optimal torsional deformation of the flapping wings. At the same time, the wind tunnel test coupled with high-speed camera technology is used to observe the deformation of “Dove” flapping wing, the optimal torsion is compared with it by calculated in different spanwise positions, so as to provide a program for the improvement of the flapping wing design.

2. Model and method

In this paper, the deformation state of the flapping wing of the carrier pigeon is analyzed by wind tunnel tests coupled with high-speed camera experiments. At the same time, numerical simulation is used to analyze the optimal torsion parameters of different spreading positions of the wing of the carrier pigeon.

2.1 Research subject

This paper focuses on the wing of the "Dove" aircraft, which has a flapping amplitude of 35°, a cruising speed of approximately 8 m/s, and a flapping frequency of about 8 Hz, as shown in Figure 1.

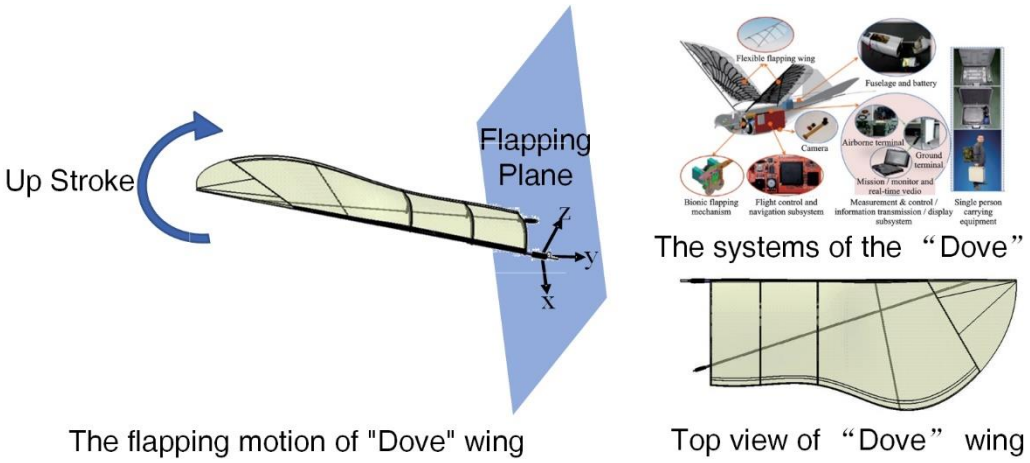

Figure 1 – “Dove” aircraft and “Dove” wing

Six spanwise positions (SP_1 ~ SP_6) are selected on the wing of the “Dove”, the distances from the flapping axis are L_1 ~ L_6, and the chord lengths of each position are c_1 ~ c_6, as shown in Figure 2, and the specific values are shown in Table 1.

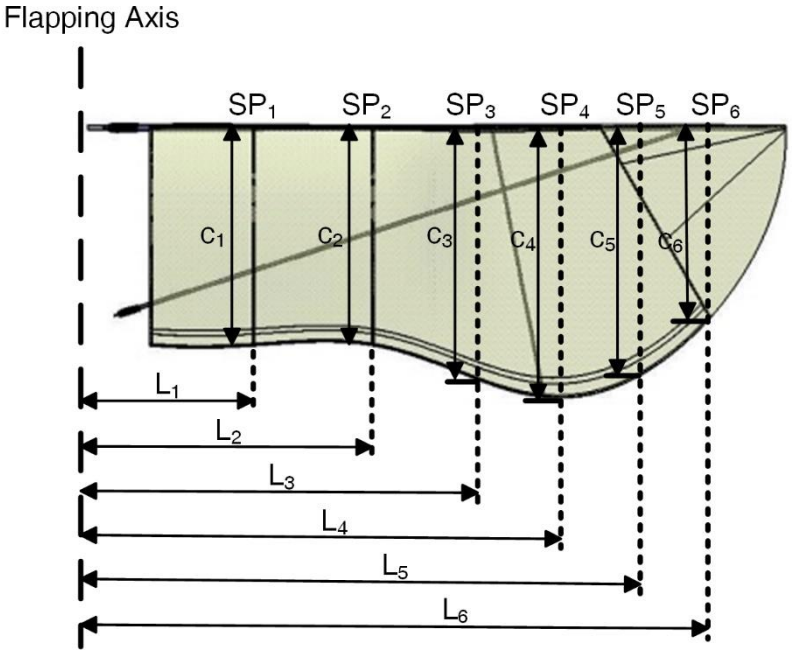

Figure 2 – Spanwise position for the “Dove” wing.

Table 1 – Distance from flapping axis and corresponding chord lengths for different spanwise positions.

Spanwise Positions	SP1	SP2	SP3	SP4	SP5	SP6
Distance from flapping axis	75 mm	130 mm	185 mm	220 mm	250 mm	285 mm
amplitude of heaving h_0	21.4 mm	79.4 mm	113 mm	134.4 mm	152.7 mm	174.1 mm
chord length	100 mm	100 mm	120 mm	125 mm	115 mm	85 mm

It is worth noting that the airfoil is not the same for the different spanwise positions of the “Dove” wing, as shown in Figure 3.

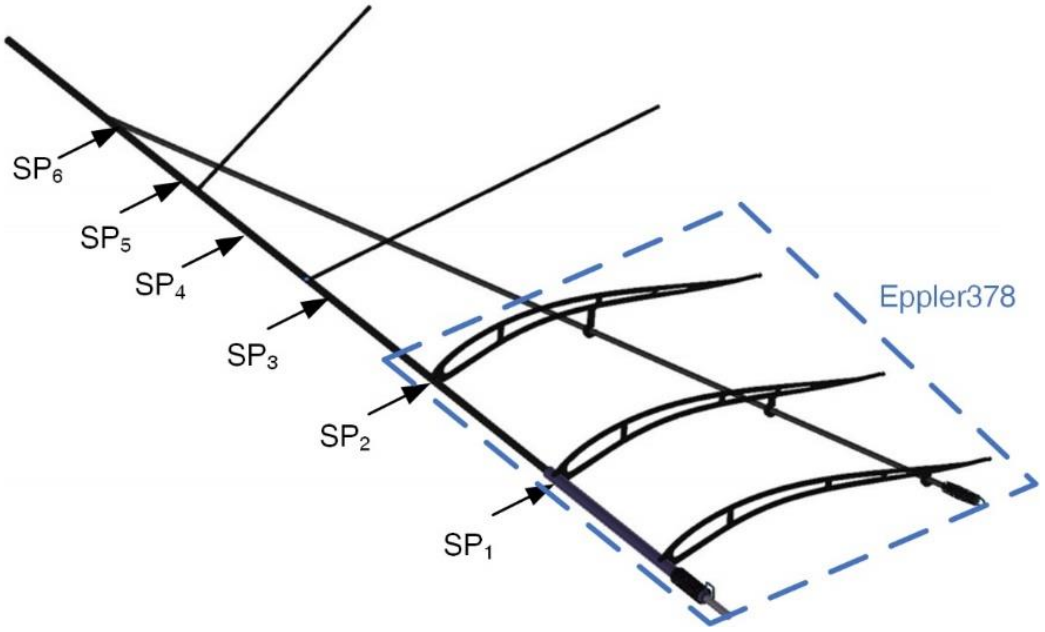

Figure 3 – Airfoil with different spanwise positions

The airfoil near the wing root is Eppler 378, while there is no specific airfoil near the wing tip. The chord length at each spanwise position is also different.

2.2 Experimental Methods

This article employs two high-speed cameras to measure the deformation parameters of flapping wings. The experimental setup is illustrated in Figure 4.

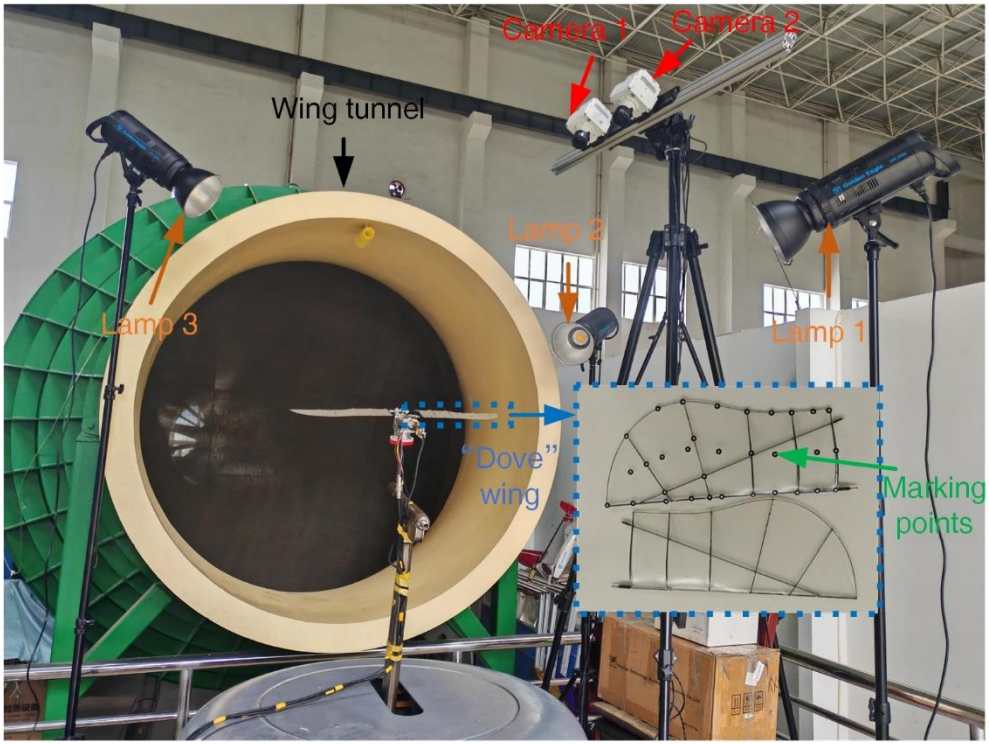

Figure 4 – The experimental setup of wind tunnel testing coupled with high-speed camera technology.

The measurement of wing deformation during flapping motion is achieved by measuring the position information of specific markers on the wing surface. Therefore, in order to ensure measurement accuracy, it is necessary to paste several markers on the wing surface, ensuring that they are sufficiently visible and of suitable size. As shown in Figure 4, the camera is positioned at a small angle to clearly capture the markers on the right wing and the body of the flapping wing. The placement of the lighting system should be as close to the experimental model as possible, providing

sufficient illumination without interfering with the model's motion or affecting the camera's capture. The camera's focal length, aperture, exposure time, and other parameters are continuously adjusted to ensure good image clarity, depth of field, and brightness. After calibration is completed, experimental photos are taken.

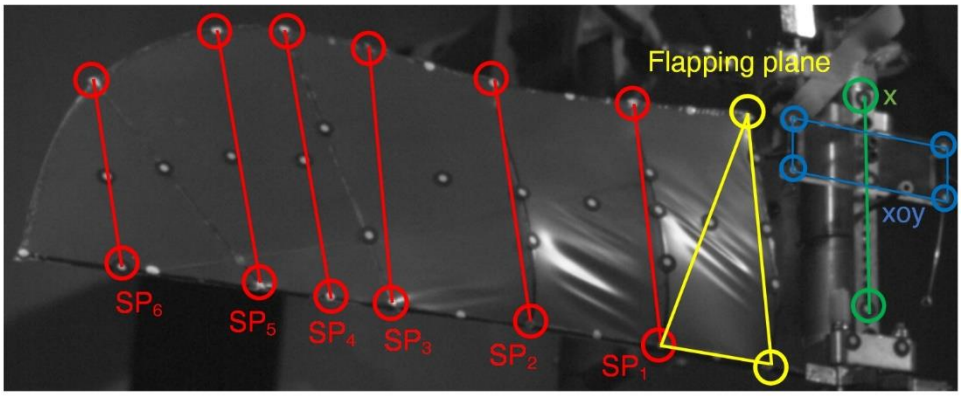

Figure 5 – Flapping wing marker point information.

In Figure 5, the red dots represent the marked points of the leading and trailing edges of the wing at various spanwise positions. The red lines indicate the corresponding spanwise positions. The green dots represent two points on the flapping mechanism. The green line formed by these two points represents the x-axis. The blue rectangle represents the horizontal plane. The yellow triangle represents the small deflection flapping plane at the wing root.

Before the experiment begins, a motion calibration board is used to collect preliminary data, which is then used to obtain the coordinate transformation matrix between the image coordinate system and the world coordinate system. The coordinate transformation matrix is used to derive the coordinates of various marker points on the wing.

Due to the greater rigidity at the wing root, smaller deformations are generated. In this paper, the angle between the plane formed by the small deformations at the wing root (represented by the yellow line in Figure 5) and the horizontal plane (represented by the blue line in Figure 5) is defined as the flapping angle. The formula for calculating the flapping angle is as follows:

$$\psi = \frac{\vec{n}_1 \bullet \vec{n}_2}{|\vec{n}_1| \bullet |\vec{n}_2|} \times \frac{180^o}{\pi} \tag{1}$$

Here, $\vec{n}_1$ represents the normal vector of the horizontal plane, and $\vec{n}_2$ represents the normal vector of the flapping plane.

The angle between the vector formed by the same string's forward edge marking point and rear edge marking point, and the x-axis, is defined as the twist angle of each station's desired position. The calculation formula is as follows:

$$\chi = \frac{\vec{x} \bullet \vec{a}}{|\vec{x}| \bullet |\vec{a}|} \times \frac{180^o}{\pi} \tag{2}$$

Here, χ represents the torsion angle, $\vec{x}$ represents the x-axis, and $\vec{a}$ represents the vector formed by the corresponding positions of the leading and trailing edge markers of the wing.

In this study, experiments will be conducted on the cruising state of the "Dove" aircraft. The incoming flow velocity will be $U_\infty = 8m/s$, and the flapping frequency will be $f = 8Hz$.

2.3 Numerical Simulation Parameters and Methods

The flapping motion generated by the movement and flexibility of the wings can be manifested as the pitching and heaving motion of the airfoil at various spanwise positions. In this paper, we will investigate the pitching and heaving motion of the airfoil at different spanwise positions, and subsequently explore the optimal twisting state of the flapping wings. The pitching and heaving motion of a two-dimensional airfoil about the leading edge is shown in Figure 6.

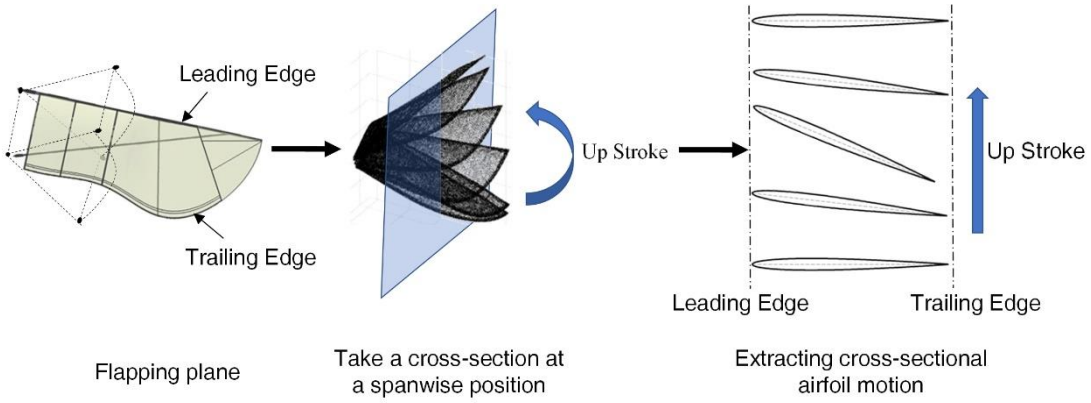

Figure 6 – The movement form of “Dove” wing in an advective position.

The heaving and pitching motion functions are as follows:

$$h = h_0 \cdot cos(2\pi ft)$$
$$\theta = \theta_0 \cdot cos(2\pi ft + \psi) \quad (3)$$

Here, h_0 is the amplitude of heaving, θ_0 is amplitude of pitching, ψ is the phase difference between heaving and pitching motions. In this paper, ψ is taken as 90°. Because this value is considered to have the best propulsive efficiency[11][12]. The heaving amplitude h_0 is affected by the flapping amplitude and the spanwise position. The specific parameters are as follows:

$$h_0 = sin(\Phi) \cdot s \quad (4)$$

Here, Φ is the flapping amplitude and s is the distance of the spanwise position from the flapping axis. The torsional motion of the “Dove” wing is considered to be around the leading edge of the wing, so the center of rotation of the pitching motion of the two-dimensional airfoil is the leading edge of the airfoil.

Another important kinematic parameter in the coupled motion of heave and pitch is the effective angle of attack $\alpha_{eff}(t)$. It is the sum of the instantaneous pitch angle $\theta(t)$ and the induced angle of attack caused by the heave motion. Therefore, for $\psi = 90^o$, the instantaneous effective angle of attack $\alpha_{eff}(t)$ is:

$$\alpha_{eff}(t) = arctan(\frac{\dot{y}_h(t)}{U_\infty}) - \theta(t) \quad (5)$$

The amplitude of the effective angle of attack is：

$$\alpha_{eff} = arctan(\frac{2\pi f h_0}{U_\infty}) - \theta_0 \quad (6)$$

In this paper, the Reynolds-averaged Navier–Stokes (RANS) method is used to solve for different kinematic states. For the feasibility and accuracy of the computational method, numerical simulations are performed to compare the experiments conducted by Heathcote[13]. The experimental model is a rectangular wing with a NACA0012 airfoil, with Reynolds number based on the chord length Re = 3×10^4. The wing undergoes harmonic heaving motion, as shown in equation (7). The geometric and motion parameters of the experimental model are shown in Table 2.

$$H = 0.175c \cdot \cos(\omega t) \quad (7)$$

Table 2 – The geometric and motion parameters of the experimental model.

Parameter	chord	Half span length	Amplitude of heaving	Heave angle frequency ω	Incoming flow velocity	Incoming flow density
Value	0.1 m	0.3 m	0.175 m	10.92 rad/s	0.303 m/s	1000 kg/m^3

Nested grids are used for the calculations, where the background grid has a grid volume of 37964 and the computational wing grid volume is 87080, for a total grid volume of about 125,000 meshes. The height of the first grid layer of the wing grid object plane is 2.0×10^{-5}, ensuring that y+ is less

than 1.0. The C_T of the calculations is shown in Figure 7. Although the calculated C_T of the flapping wing shows some differences from the experimental values, compared to the calculations of Liu[14], the calculation method used in this paper better captures the phase of the two thrust peaks in the experimental results, verifying the credibility of the numerical simulation method used in this paper.

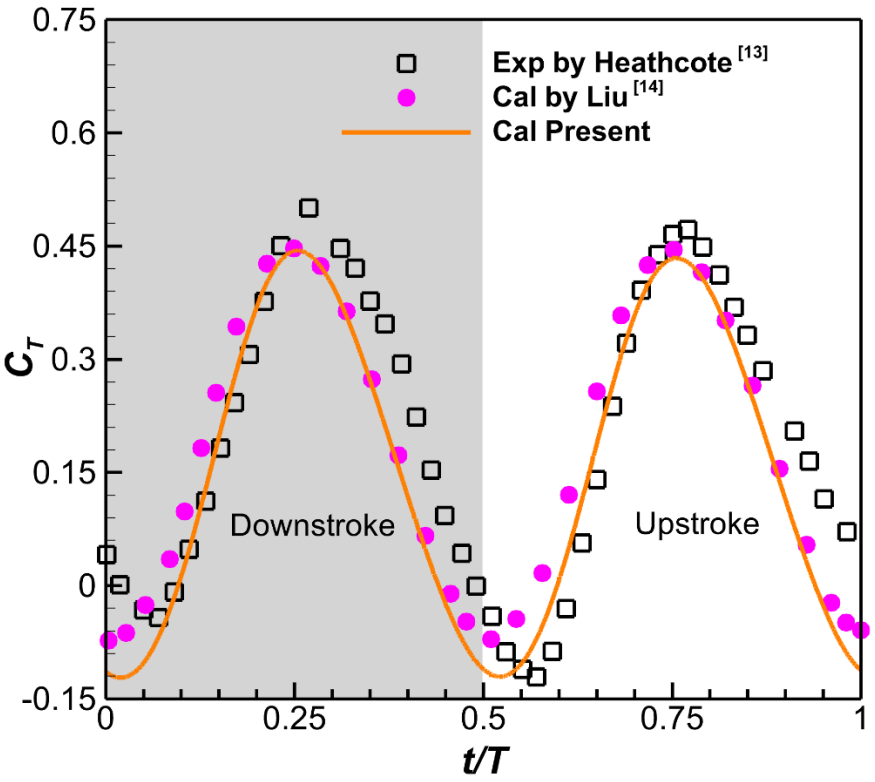

Figure 7– Comparison of instantaneous C_T calculations with experimental and others' results.

Through the non-steady motion case of the airfoil, the feasibility of using a dynamically nested mesh for flapping dynamics has been verified. At the same time, it also demonstrates that the numerical simulation method employed has good accuracy for non-steady calculations of low Reynolds number flapping.

To ensure the accuracy of subsequent calculations and avoid the influence of grid resolution and time step size on the calculation results, we investigate the effects of three types of grid resolution (Coarse, Medium, and Precision) and three timestep sizes (large, medium, and small). The specific parameters are shown in Table 3. The grid resolutions for the three types of grids are 6×10^4, 1.2×10^5, and 2.4×10^5, respectively. The computational state is chosen as Re = 8.8×10^4, and the amplitude of the heaving is h_0 = 700 mm and the amplitude of the pitching is 5°, and the amplitude of the pitching motion is carried out.

Table 3 – Comparison of Different Grid Types and Time Step Length Results.

The influence of grid resolution					
Grid Resolution	Time Step	$C_{L,mean}$	$\lvert\triangle C_{L,mean}\rvert$	$C_{D,mean}$	$\lvert\triangle C_{D,mean}\rvert$
Coarse Mesh	$\Delta t = T/1250$	0.40678	\	-0.35474	\
Medium Mesh	$\Delta t = T/1250$	0.44757	10.0275%	-0.35346	0.3608%
Precision Mesh	$\Delta t = T/1250$	0.44622	0.3016%	-0.35264	0.2320%
The influence of time step					
Grid Resolution	Time Step	$C_{L,mean}$	$\lvert\triangle C_{L,mean}\rvert$	$C_{D,mean}$	$\lvert\triangle C_{D,mean}\rvert$
Medium Mesh	$\Delta t = T/625$	0.46913	\	-0.35022	\
Medium Mesh	$\Delta t = T/1250$	0.44757	4.5957%	-0.35346	0.9251%
Medium Mesh	$\Delta t = T/2500$	0.44173	1.3048%	-0.35548	0.5715%

Considering computational accuracy and cost-effectiveness, the subsequent simulations will be conducted using a medium mesh and a time step of $\Delta t = T/1250$.

3. Result and discussion

3.1 Experiment

After completing the experiment for "Dove" wing cruise state and collecting experimental photos, we used the open-source digital tool DLTdv8 developed by Hedrick[15] to track the positions of wing surface and fuselage markers in each frame of the captured footage. Calculate the spatial position of marker points based on the Direct Linear Transform (DLT) method, and provide the corresponding three-dimensional coordinates of the marker points in the measurement coordinate system. This allows obtaining the three-dimensional coordinate values of any marker point at each sampling moment.

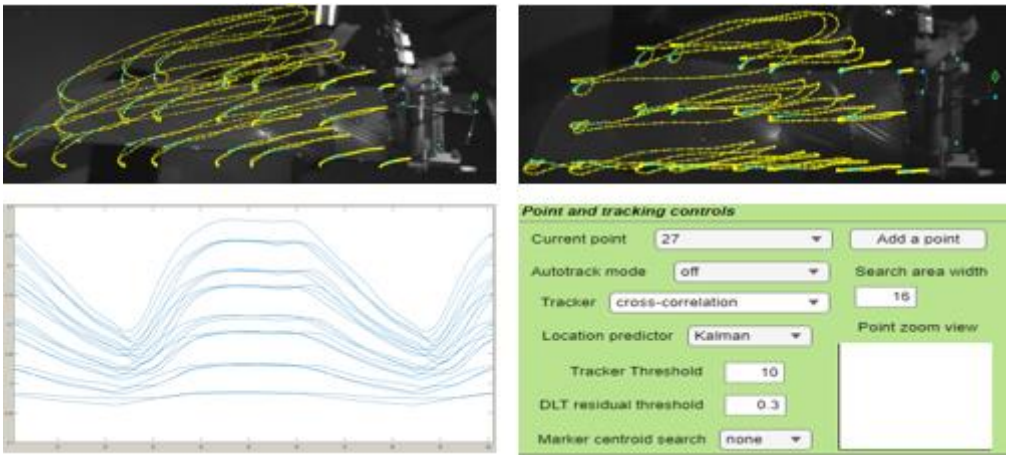

Figure 8 – DLTdv8 Marker Point Tracking.

The deformation of the wing is parameterized as the local flapping angle and torsion angle at different spanwise stations. The definition and calculation method are shown in Eq.(1) and Eq.(2).

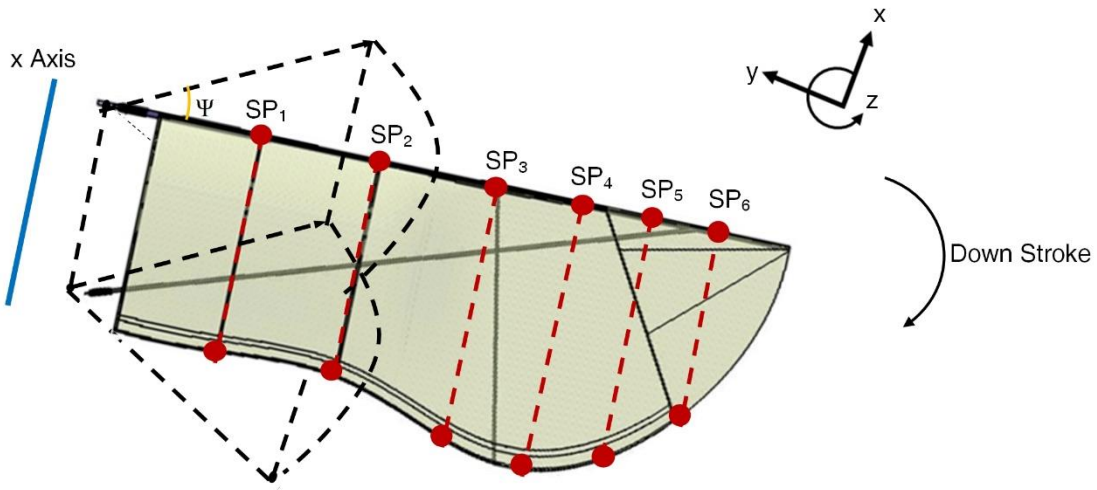

Figure 9 – Flapping angle and calculated torsion angle position.

The experimentally obtained flapping angle and torsion angles for each spanwise position are given in Figure 10. A sixth-order Fourier function was used to fit the angles.

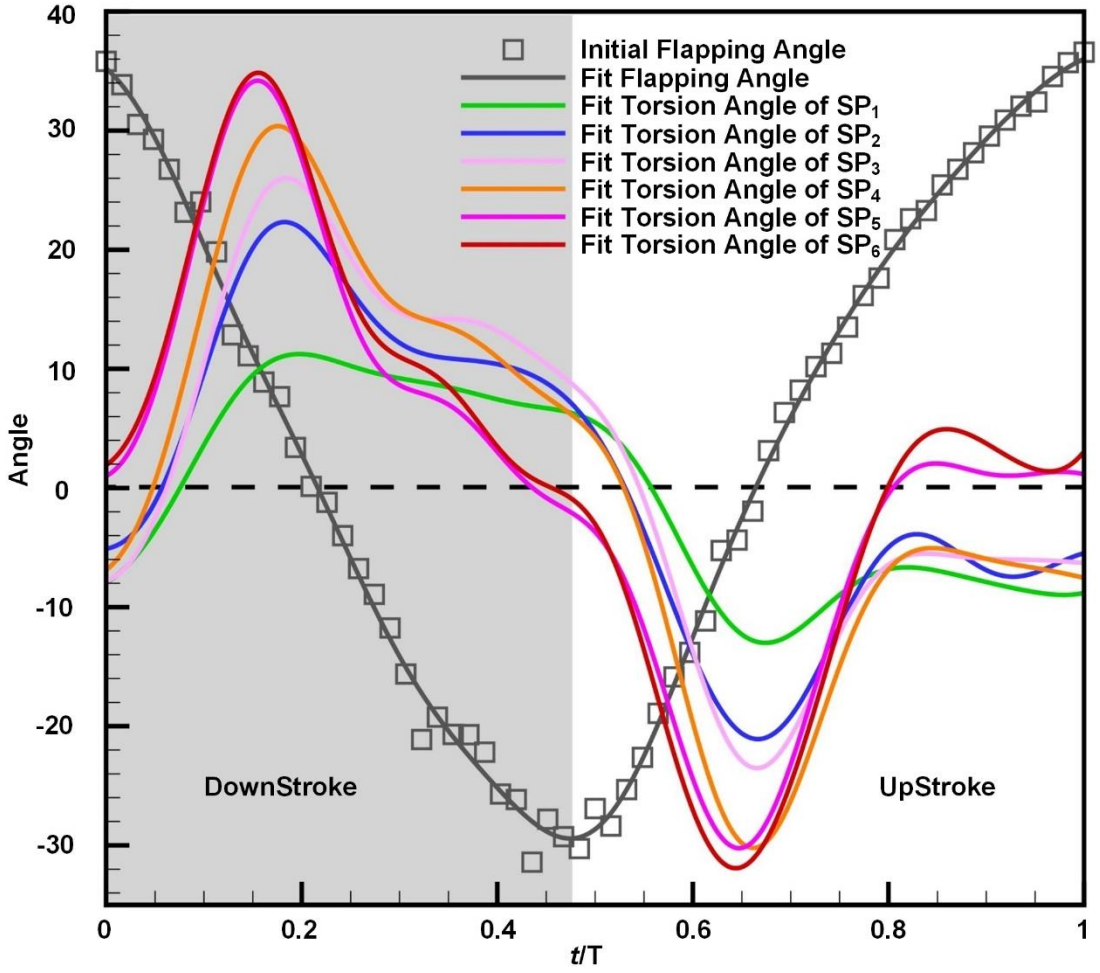

Figure 10 – Instantaneous changes in flapping angle and torsion angle for each spanwise position.

The maximum deformation magnitude of the upstroke and downstroke for each spanwise position is shown in Table 4.

Table 4 – Maximum torsion angle for each spanwise position.

Spanwise Position	Maximum angle of twist for downstroke	Moment of maximum torsion angle of downstroke	Maximum angle of twist for upstroke	Moment of maximum torsion angle of upstroke
SP_1	11°	$t/T = 0.175$	13°	$t/T = 0.683$
SP_2	23°	$t/T = 0.175$	21°	$t/T = 0.667$
SP_3	26°	$t/T = 0.191$	23°	$t/T = 0.683$
SP_4	30°	$t/T = 0.191$	30°	$t/T = 0.667$
SP_5	32°	$t/T = 0.191$	32°	$t/T = 0.698$
SP_6	34°	$t/T = 0.191$	35°	$t/T = 0.667$

It is found that the maximum deformation at each spanwise position in the upstroke and downstroke is earlier than the middle moment. This is caused by the inertia force of the wing with a certain mass. Meanwhile, the closer the spanwise position is to the wing tip, the larger the maximum deformation is. It is worth noting that the experimental results show that the upstroke and downstroke of the “Dove” wing are not completely symmetrical. At the same time, at the maximum and minimum flapping angle, the twist angle near the root of the wing has a certain angle. This is due to the effect of the flapping mechanism.

3.2 Numerical simulation

3.2.1 Calculation of optimal torsion angle

In this paper, the kinematic states for obtaining the maximum thrust are calculated for the Eppler 378 and NACA0002 airfoils in different states. The calculated states are determined by the parameters

and spanwise positions of the “Dove” wing.

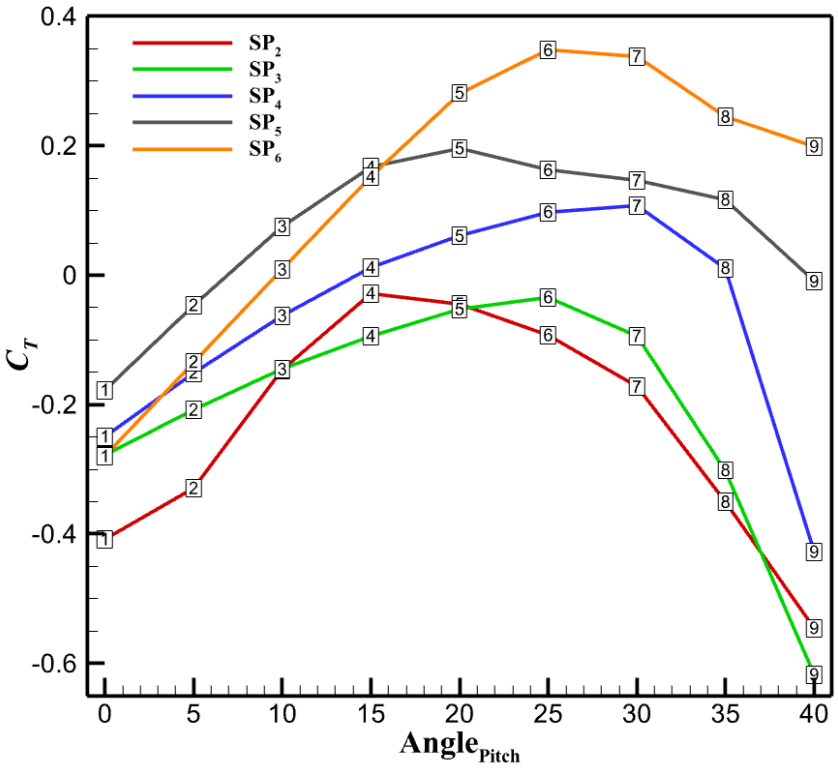

Figure 11 – Variation of C_T with pitching amplitude for different spanwise positions.

The variation of the wing C_T with pitching amplitude for each spanwise position of the “Dove” wing SP_1-SP_6 is given in Figure 11. The optimum pitch angle exists for the thrust to reach its peak value. We refer to the pitch angle corresponding to the case of maximum thrust as the optimal pitch angle Its peak occurrence state is shown in Table 5.

Table 5 – Comparison of Optimal Pitch Angle with different spanwise positions.

Spanwise Position	SP_1	SP_2	SP_3	SP_4	SP_5	SP_6
Distance from flapping axis	75 mm	130 mm	185 mm	220 mm	250 mm	285 mm
Chord length	100 mm	100 mm	120 mm	125 mm	115 mm	85 mm
Current twist angle	11°	23°	26°	30°	32°	35°
Optimum pitch angle	10°	15°	25°	30°	20°	25°

Comparing the optimal torsion state with the maximum thrust and the current torsion state of the “Dove” wing, it can be found that the torsion amplitude near the wing root is closer to the optimal torsion amplitude, but the torsion deformation near the wing tip is too large. It is worth noting that this paper adopts a 5° step of pitching amplitude for the calculation, and the calculation results only consider the aerodynamic force, which lacks the consideration of inertial force. Although the results have some errors, they still have some reference value.

3.2.2 Effect of different kinematic parameters

From the existing calculations, it is known that the optimal pitch angle will increase with the increase of the motion amplitude, and at the same time, the optimal pitch angle will decrease with the decrease of the chord length. In order to have a clearer understanding of the effect of each motion parameter on the optimal pitch angle. We analyze the effects of different frequencies, incoming velocities, and heaving amplitudes.

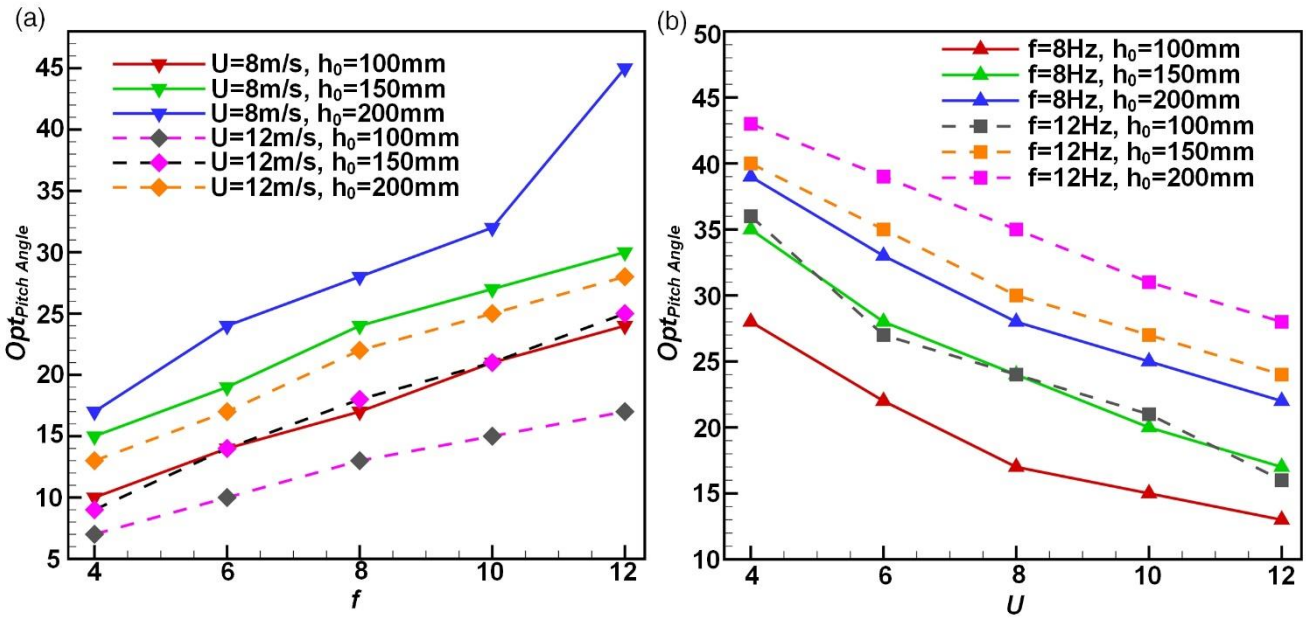

Figure 12 – Variation of optimal pitch angle with heaving amplitude for different frequencies and incoming velocities.

The results in Figure 12 show that the optimal pitch angle increases as the heaving amplitude and frequency increase or the incoming velocity decreases.

The magnitude of the effective angle of affect affects the thrust performance of the airfoil, and the thrust will decrease when the effective angle of attack is too large or too small. The amplitude of the effective angle of affects, $\alpha = arctan(\frac{2\pi f h_0}{U_\infty}) - \theta_0$, can be found to increase with an increase in heaving amplitude and frequency or a decrease in the incoming velocity if the pitching amplitude θ_0 is kept constant. In order to avoid excessive effective angle of attack, the optimal pitch angle will increase with increasing heaving amplitude and frequency, or with decreasing incoming velocity.

4. Conclusion

In this paper, the experimental study of the “Dove” wing is carried out by using high-speed camera technology, and the torsional states of six different spreading positions of SP_1-SP_6 are obtained by using the direct linear transformation (DLT) method. The experimental results show that the farther the spanwise position from the flapping axis, the larger the torsional deformation it produces. In addition, the torsional peak occurs before the middle moment of the downstroke and upstroke due to the effect of inertial forces present in the wing. The geometrical and kinematic parameters of the selected spanwise positions SP_1-SP_6 of the “Dove” wing are extracted in order to achieve a greater thrust performance of the wing. The RANS method is used to calculate the heaving and pitching motion with different pitch amplitudes for airfoils at each spanwise position. Comparing the calculation results of different pitch amplitudes, the pitch amplitude corresponding to the maximum thrust generated is defined as the optimal pitch angle. Comparing the torsional state of the current “Dove” wing with the optimal pitch angle obtained from numerical simulation, it is found that the torsional deformation near the wing root is closer to the optimal pitch angle, and the torsional deformation near the wing tip is too large. Therefore, the current stiffness distribution of the “Dove” near the wing root is more appropriate, and the stiffness at the wing tip needs to be increased appropriately to reduce the torsional amplitude at the wing tip.

In this paper, the effects of incoming velocity, frequency and heaving amplitude on the optimum pitch angle are investigated and it is found that frequency and heaving amplitude are positively correlated with the optimum pitch angle, while incoming velocity is negatively correlated with the optimum pitch angle. It is worth noting that the incoming velocity, frequency, heaving and pitching amplitude together control the magnitude of the effective angle of affect. The variation of the optimum pitch angle with the incoming velocity, frequency and heaving amplitude can avoid the effective angle of affect amplitude being too large or too small and thus maximize the thrust acquired.

5. Contact Author Email Address

Mailto: xuedong@nwpu.edu.cn

6. Copyright Statement

References

[1] Baier D.B., Gatesy S.M. and Dial K.P. Three-dimensional, high-resolution skeletal kinematics of the avian wing and shoulder during ascending flapping flight and uphill flap-running. *PLoS One*, Vol. 8, 2013.

[2] Xuan J.L., Song B.F. Song W.P. et al. The research progress of the Chinese “Dove” flapping wing aircraft and the future development of bird flight mechanisms and application systems. *Transactions of Nanjing University of Aeronautics and Astronautics.* Vol. 37, N0. 5, pp 5-11, 2020.

[3] Send W, Fischer M, Jebens K, et al. Artificial hinged-wing bird with active torsion and partially linear kinematics. *Congress of the International Council of the Aeronautical Sciences*. 2012.

[4] Jiao Z, Zhao L, Shang Y, et al. Generic Analytical Thrust-Force Model for Flapping Wings. *AIAA Journal*, Vol. 56, No 2, pp 581-593, 2018.

[5] Chowdhury J. and Ringuette M.J. A simple vortex-loop-based model for unsteady rotating wings. *Journal of Fluid Mechanics*, Vol 880, No 43, pp 1020-1035, 2019.

[6] Küssner, H.G. Zusammenfassender Bericht über den instationären Auftrieb von Flügeln. *Luftfahrtforschung.* Vol 13, No 12, pp 410–424, 1936.

[7] Theodorsen, T. General Theory of Aerodynamic Instability and the Mechanism of Flutter, *NACA Annual Rept*. pp 413–433, 1949.

[8] Lu K, Xie Y H and Zhang D. Numerical study of large amplitude, nonsinusoidal motion and camber effects on pitching airfoil propulsion. *Journal of Fluids and Structures*, Vol 36, No 1, pp 184-194, 2013.

[9] Lagopoulos N S, Weymouth G D and Ganapathisubramani B. Universal scaling law for drag-to-thrust wake transition in flapping foils. *Journal of Fluid Mechanics*, Vol 872, No R1, pp 1-11, 2019.

[10] Fernandez-Feria R. Note on optimum propulsion of heaving and pitching airfoils from linear potential theory. *Journal of Fluid Mechanics*, Vol 826, No 30, pp 781-796, 2017.

[11] Max F.P, and Kevin D.J. Flapping wing aerodynamics-progress and challenges. *AIAA Journal*. Vol 46, No 9, pp 2136-2149, 2008.

[12] Yuan W, Lee R, Hoogkamp E and Khalid M. Numerical and Experimental Simulations of Flapping Wings. *International Journal of Micro Air Vehicles*. Vol 2, No 3, pp 181-209, 2010.

[13] Heathcote S., Wang Z., Gursul I. Effect of spanwise flexibility on flapping wing propulsion[J]. Journal of Fluids and Structures, 2008, 24(2): 183-199.

[14] Liu H. Integrated modeling of insect flight: From morphology, kinematics to aerodynamics[J]. Journal of Computational Physics, 2009, 228(2): 439-459.

[15] Hedrick T L. Software techniques for two-and three-dimensional kinematic measurements of biological and biomimetic systems. *Bioinspiration & biomimetics*, Vol 3, No 3, pp 34-40, 2008.